Mesoporous silica nanoparticle-based protein delivery systems for biomedical applications

Tu, J.

Chapter III

Mesoporous Silica Nanoparticle-Coated Microneedles for Intradermal Delivery of Ovalbumin

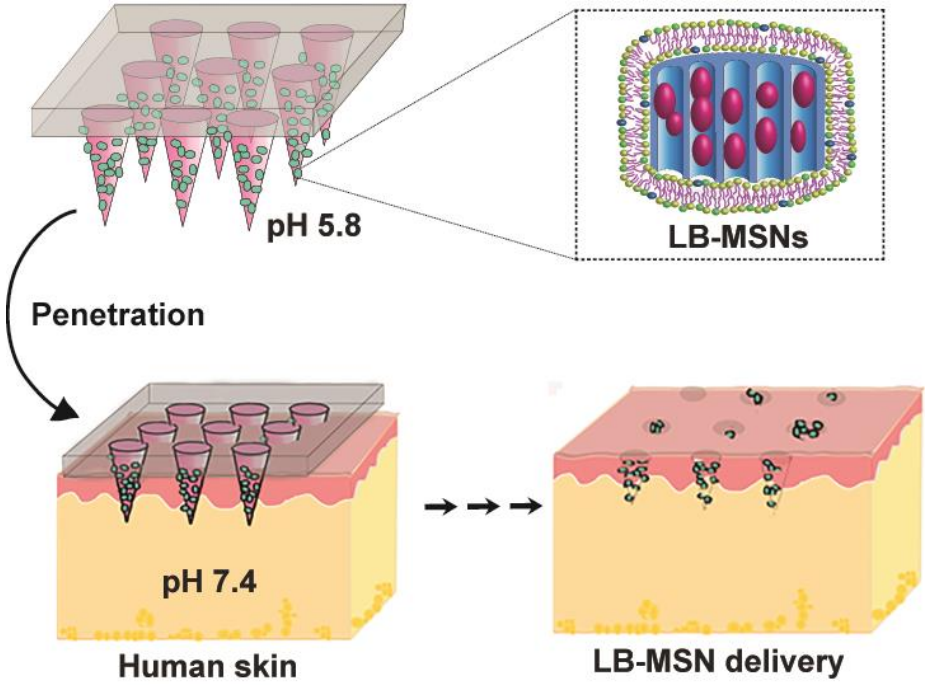

Jing Tu, Guangsheng Du, M. Reza Nejadnik, Juha Mönkäre, Koen van der Maaden, Paul H. H. Bomans, Nico A. J. M. Sommerdijk, Wim Jiskoot, Joke A. Bouwstra, and Alexander Kros

Abstract

Herein we report a new intradermal delivery system by coating pH-sensitive microneedles with antigen-loaded, lipid bilayer-covered MSNs. A novel type of ultrafine MSNs with large pores (~10 nm in diameter) was synthesized with a positive surface charge, resulting in efficient loading of ovalbumin (OVA) in the MSN pores (AEP-MSNs). A lipid bilayer (LB) was assembled at the MSN surface to enhance the colloidal stability (LB-MSNs). The designed LB-MSNs were coated onto pH-sensitive pyridine modified microneedles by electrostatic interactions between the modified silicon surface and the LB-MSNs at low ionic strength. The presence of LB-MSNs on the surface of pyridine modified microneedles was confirmed by both scanning electron microscopy (SEM) and confocal laser scanning microscope (CLSM). The delivery of LB-MSNs into *ex vivo* human skin was studied. This designed microneedle-mediated intradermal delivery system for mesoporous nanoparticles could be a promising tool to deliver a wide range of compounds into the skin. The method is not restricted to the delivery of antigens, but can also be used to deliver any compound that can be encapsulated in MSNs like (low-molecular-weight) drugs, RNA/DNA and proteins.

Keywords: Intradermal antigen delivery, lipid bilayer, mesoporous silica nanoparticles, pH-sensitive microneedles

3.1 Introduction

Vaccination is regarded as one of the most promising strategies for reducing mortality and improving human health.[1, 2] Most of the current vaccines are delivered by intramuscular or subcutaneous injection, but the inherent limitations are obvious, such as the risk of the needle-related disease induced by reusing needles and syringes, the needle fear by children and patients, and the need for maintaining a proper cold chain during storage and transport.[1, 2] Therefore, new needle-free, easy to use and effective vaccination methods are urgently needed. One of these potential methods is microneedle-mediated intradermal vaccination.[3]

Intradermal vaccination is attractive because the skin is easily accessible and the large number of immune cells inside the skin, such as dendritic cells (DCs), make the skin promising for vaccination.[1, 4-6] Microneedles are micron-sized structures with a length of less than 1 mm which can be used to overcome the skin barrier located in the top layer of the skin. Microneedles enable minimally-invasive and potentially pain free delivery of vaccine into skin.[5-8 9, 10] Previously, in our lab we designed pH-sensitive pyridine modified microneedles with a surface pK_a below physiological pH, which allows the adsorption of negatively-charged proteins at slightly acidic conditions (pH 5.8) and the release at neutral pH (pH 7.4). We studied the immunization of mice by using ovalbumin (OVA) coated pH-sensitive microneedles.[8, 11] It was found that microneedle-mediated immunization led to comparable T-cell responses but lower IgG responses as conventional subcutaneous or intradermal immunization. Possible strategies to further improve the immunogenicity of vaccines by the intradermal route could be adding an adjuvant or using nanoparticles to deliver the antigens.[2, 8, 12-17]

To improve the uptake of antigens by DCs and elicit a more potent immune response, antigens can be formulated into nanoparticles.[13, 18] The adjuvanticity of nanoparticles is attributed to their capability of protecting antigen from degradation, forming a depot at the site of injection, and facilitating antigen uptake by DCs.[19] A variety of nanosized vaccine delivery systems have been developed, such as polymeric nanoparticles,[20] emulsions,[21] and lipid-based nanoparticles.[19, 20, 22] Recently mesoporous silica nanoparticles (MSNs) have gained significant attention as drug delivery vehicles because of their large surface area and large pore volume for the loading of active small molecules or proteins, controlled size and mesostructure, and excellent *in vivo* biocompatibility.[2, 23-32]

Herein, we report a new intradermal delivery system, which synergistically integrates the advantages of nanoparticles and microneedles, by coating pH-sensitive microneedles with

antigen-loaded, lipid bilayer-covered MSNs. OVA was used as model antigen that is negatively charged (pI of 4.9)[33] at pH 7.4. For the delivery of proteins, a novel type of ultrafine MSNs with large pores (~10 nm in diameter) was synthesized with a positive surface charge, resulting in efficient loading of OVA in the MSN pores (AEP-MSNs). To enhance the colloidal stability of OVA loaded AEP-MSNs, a lipid bilayer (LB) was assembled at the MSN surface and the lipid-coated MSNs are referred to as LB-MSNs.[34-37] This method synergistically combines features of liposomes and MSNs and has been reported to address the multiple challenges, like stability, targeting and multicomponent delivery.[35-37] The designed LB-MSNs were coated onto pH-sensitive pyridine modified microneedles by the electrostatic interactions between the modified silicon surface and the LB-MSNs at low ionic strength. Piercing the LB-MSNs coated microneedles into *ex vivo* human skin resulted in the successful release of the nanoparticles due to a shift in pH from 5.8 to 7.4 (Scheme 3.1).

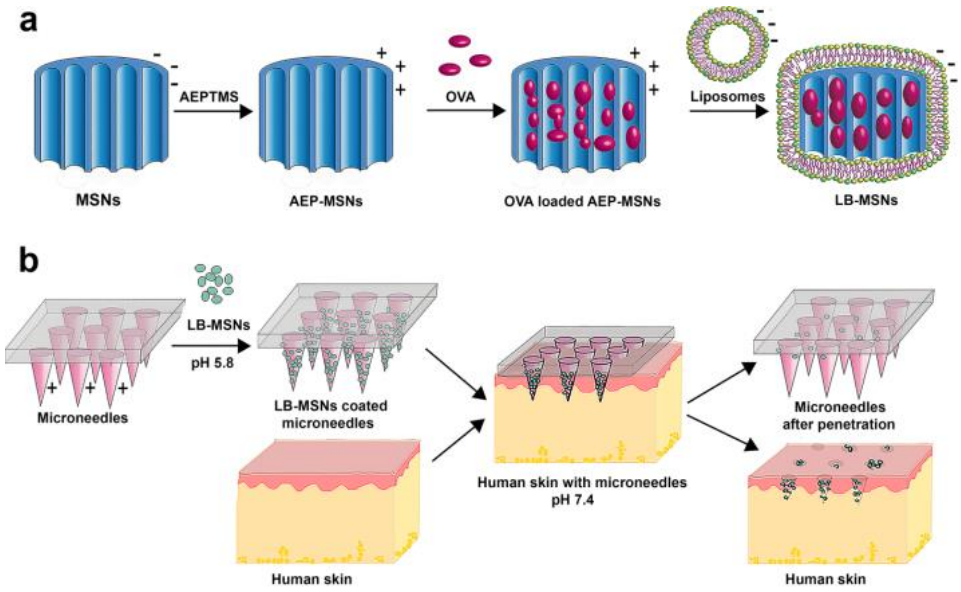

Scheme 3.1 *Preparation and application of pH-sensitive microneedle arrays coated with LB-MSNs. (a) Encapsulation of OVA into AEP-MSNs, followed by fusion of liposomes (composed of DOPC/DOPS/cholesterol), resulting in LB-MSNs. (b) Adsorption of LB-MSNs onto pH-sensitive microneedles and penetration of microneedles into human skin, resulting in a pH shift and delivery of LB-MSNs into the viable epidermis and dermis.*

3.2 Materials and Methods

3.2.1 Materials

Tetraethyl orthosilicate (TEOS), ethanol, acetone, methanol, isopropanol, sulfuric acid (96-98%), acetic acid, hydrochloric acid (36%-38%), (3-aminopropyl)triethoxysilane (APTES), 4-pyridinecarboxaldehyde, sodium cyanoborohydride, 3-[2-(2-aminoethylamino)ethylamino] propyltrimethoxysilane (AEPTMS), Ovalbumin (OVA), 1,3,5-trimethylbenzene (TMB), Pluronic P123 and cholesterol were purchased from Sigma-Aldrich. Fluorocarbon surfactant FC-4 was purchased from Yick-Vic Chemicals & Pharmaceuticals (HK) Ltd. 1,2-dioleoyl-sn-glycero-3-phosphocholine (DOPC), 1,2-dioleoyl-sn-glycero-3-[phosphor-$_L$-serine](sodium salt) (DOPS), and 1,2-dioleoyl-sn-glycero-3-phosphoethanolamine-N-(lissamine rhodamine B sulfonyl) (ammonium salt) (DOPE-LR) were purchased from Avanti Polar Lipids Inc. Hydrogen peroxide (30%) and ethylenediaminetetraacetic acid (EDTA) were purchased from Fluka. Toluene was purchased from Biosolve. Alexa Fluor®488 ovalbumin conjugates (OVA-AF488) was purchased from Thermo Fisher Scientific. Sterile phosphate buffered saline (PBS, 163.9 mM Na^+, 140.3 mM Cl^-, 8.7 mM HPO_4^{2-}, 1.8 mM $H_2PO_4^-$, pH 7.4) was obtained from Braun. All reagents were used without further purification. Milli-Q water (18.2 MΩ/cm, Millipore Co., USA) was used for the preparation of solutions. 1 mM phosphate buffer (PB) with a pH of 7.4 was prepared in the lab. Silicon microneedle arrays with 576 microneedles per array on a back plate of 5 × 5 mm^2 and a length of 200 μm per microneedle were kindly provided by Bosch.

3.2.2 Preparation of mesoporous silica nanoparticles (MSNs) with large ordered mesochannels

MSNs were synthesized according to a published procedure[38] with modifications.[39] Briefly, surfactant Pluronic P123 (0.5 g) and FC-4 (1.4 g) were dissolved in HCl (80 mL, 0.02 M), followed by the introduction of TMB (0.48 mL). After stirring for 6 h, TEOS (2.14 mL) was added dropwise. The resulting mixture was stirred at 30 °C for 24 h and transferred to an autoclave at 120 °C for 2 days. Finally, the solid product was isolated by centrifugation, and washed with ethanol and Milli-Q water. The organic template was completely removed by calcination at 550 °C for 5 h.

3.2.3 Synthesis of amino-functionalized MSNs (AEP-MSNs)

To prepare cationic MSNs, AEPTMS in absolute ethanol (4 mL, 20 wt%) was incubated with MSNs (100 mg) overnight at room temperature. The desired AEP-MSNs were collected by centrifugation and washed with ethanol to remove unreacted AEPTMS.

3.2.4 Encapsulation of OVA in AEP-MSNs

To determine the encapsulation kinetics of OVA in AEP-MSNs, AEP-MSNs (0.5 mL, 2 mg/mL) and OVA (0.5 mL, 0.5 mg/mL) were mixed and incubated in Eppendorf mixer (400 rpm, 25 °C) for different time period (0, 0.5, 1, 2, 4, 8 and 24 h). After incubation, the suspensions were centrifuged and the encapsulation efficiency (EE%) of OVA was determined by measuring the difference in its intrinsic fluorescence intensity with a plate reader (Tecan M1000) (excitation wavelength = 280 nm and emission wavelength = 320 nm) in the supernatant before and after the encapsulation.

To determine the maximum loading capacity (LC%) of OVA in AEP-MSNs, AEP-MSNs (2 mg/mL) were mixed with different initial concentrations of OVA (ranging from 0.25, 0.5, 1, 1.5, 2 to 3 mg/mL) and incubated in an Eppendorf mixer (400 rpm, 25 °C) for 0.5 h. Next, the suspensions were centrifuged at 9000 g for 5 min. The EE% of OVA was determined by measuring the difference in their intrinsic fluorescence intensity in the supernatant before and after the encapsulation with a plate reader (Tecan M1000). The EE% and LC% were calculated as below: [19, 40]

$$\text{EE } \% = \frac{t_{ova} - f_{ova}}{t_{ova}} \times 100\ \% \tag{3.1}$$

$$\text{LC } \% = \frac{t_{ova} - f_{ova}}{OVA\ loaded\ AEP\text{-}MSNs} \times 100\ \% \tag{3.2}$$

Where t_{ova} represents the total content of OVA, and f_{ova} is the content of free OVA (OVA in the supernatant).

3.2.5 Preparation of liposomes

Liposomes were prepared by dispensing stock solutions of DOPC (70 µl, 25 mg/mL), DOPS (20 µl, 12.5 mg/mL) and cholesterol (10 µl, 25 mg/mL) into scintillation vials. All lipids were dissolved in chloroform. A lipid film was created by slow evaporation of chloroform in the vial under a nitrogen flow and dried in vacuum overnight. The lipid film was rehydrated by the addition of PB (1 mL, 1 mM, pH 7.4) and the mixture was vortexed for 10 seconds to form a cloudy lipid suspension. The obtained suspension was sonicated in a water bath for 10 min. The resulting clear liposomes dispersions were stored at 4 °C. To

obtain fluorescent liposomes, a fluorescently labeled lipid (DOPE-LR) was incorporated into the liposomes by adding the lipids at 1 wt% DOPE-LR to make to the lipid solution prior to liposome formation.

3.2.6 Preparation of LB-MSNs

To prepare LB-MSNs, OVA (0.5 mL, 0.25 mg/mL) solution in PB (1 mM, pH 7.4) was first transferred into a 2-mL Eppendorf tube, followed by the addition of AEP-MSNs suspension (0.5 mL, 1 mg/mL) and liposome solution (0.5 mL, 2 mg/mL). The resulting mixture was incubated in the Eppendorf mixer for 1.5 h (400 rpm, 25 °C). The particles were collected and excess liposomes and OVA were removed by centrifugation (9000 g, 5 min). The encapsulation of OVA was determined by measuring the difference in their intrinsic fluorescence intensity in the supernatant before and after the encapsulation on a Tecan M1000 plate reader. All experiments were performed in triplicate.

3.2.7 Characterization of MSNs, AEP-MSNs and LB-MSNs

Transmission electron microscopy (TEM) images were collected by using a JEOL 1010 instrument with an accelerating voltage of 70 kV. Nitrogen adsorption-desorption isotherms were obtained with a Micromeritics TriStar II 3020 surface area analyzer. Before each measurement, MSNs were outgassed in the vacuum (below 0.15 mbar) at 300 °C for 16 h, while AEP-MSNs were outgassed at room temperature. The specific surface areas were calculated from the adsorption data in the low pressure range using the Brunauer-Emmett-Teller (BET) model.[41] The pore size distribution was determined following the Barrett-Joyner-Halenda (BJH) model.[42] The hydrodynamic size distribution and zeta-potential of the samples were measured with a Malvern Nano-zs instrument. Nanoparticle tracking analysis (NTA) measurement was performed by using a NanoSight LM20 (NanoSight, Amesbury, United Kingdom). The software used for capturing and analyzing the data was the NTA 2.0 Build 127. Thermogravimetric analysis (TGA) was conducted with a Perkin Elmer TGA7. All the samples were tested under an air atmosphere from 25 °C to 800 °C at a heating rate of 10 °C/min.

Sample vitrification for Cryo-TEM was carried out using an automated vitrification robot (FEI Vitrobot™ Mark III). Sample supports, type R2/2 Quantifoil Jena, were purchased from Quantifoil Micro Tools GmbH and contained a carbon support film on a copper grid. Prior to use the TEM grids were glow discharged by a Cressington 208 carbon coater to render them hydrophilic. Cryo-samples were prepared from a 3 μL droplet of sample solution placed on

the grid inside the Vitrobot™ chamber at 100% relative humidity and temperature of 20 °C, after which it was blotted to remove excess solution and subsequently plunged into liquid ethane for vitrification. Imaging performed using a FEI CryoTitan operating at 300 kV and equipped with a field emission gun (FEG) using low dose procedures.[43]

3.2.8 OVA release studies from AEP-MSNs and LB-MSNs

To study the influence of ionic strength on the release of OVA from AEP-MSNs, Phosphate buffer (PB, 1 mM Na_2HPO_4 and 1 mM NaH_2PO_4 were mixed at molar ratio of 5:2, pH 7.4) with various concentrations of NaCl (0, 0.9, 1.8, 3.6, 7.2, 14.4 and 28.8%, m/v) were prepared. OVA loaded AEP-MSNs (1 mg, based on the mass of AEP-MSNs) were dispersed in one of the buffers (1 mL) mentioned above. The suspensions were kept in the Eppendorf mixer for 0.5 h (400 rpm, 37 °C) and followed by centrifugation (9000 g, 5 min) to collect the supernatant. The amount of released OVA in the buffer was quantified by measuring the intrinsic fluorescence intensity of OVA with a Tecan M1000 plate reader. The released OVA in PB with 0.9, 1.8 and 3.6% NaCl was also tested by high pressure size-exclusion chromatography (HP-SEC). Far-UV circular dichroism (CD) spectra of OVA before and after release were measured by using a Jasco J-815 spectropolarimeter. Spectra were collected from 260 – 190 nm, at 25 °C.

To compare the *in vitro* release of OVA from AEP-MSNs and LB-MSNs, OVA loaded AEP-MSNs and LB-MSNs were dispersed in PBS (pH 7.4) and incubated in the Eppendorf mixer (400 rpm, 37 °C). At various time points, the suspensions were centrifuged and the supernatants were replaced with fresh PBS. The amount of OVA released into the supernatant was determined by measuring the intrinsic fluorescence intensity of OVA on a Tecan M1000 plate reader.

3.2.9 Modification of silicon microneedle arrays to obtain pH-sensitive surface

To coat negatively charged particles onto silicon microneedle arrays, the microneedles were chemically modified to obtain a pH sensitive surface (positively charged at pH 5.8) by using pyridine groups, as described previously.[44] The surface of silicon was first cleaned by acetone and methanol. Next the surfaces were hydroxylated by a fresh piranha mixture consisting of 30 % (v/v) H_2O_2 and 70 % (v/v) H_2SO_4. Then the surface was incubated with 2 % (v/v) APTES in toluene overnight at room temperature to obtain the amine modified silicon surface.

The amine modified surface was modified with 4-pyridinecarboxaldehyde (100 mM) in anhydrous isopropanol with acetic acid (1%, v/v) at room temperature. The obtained imine bonds on pyridine-modified surface were reduced to a secondary amine by incubating in $NaBH_3CN$ (50 mM) in isopropanol for 2 h. Finally the modified surface was cleaned with isopropanol and methanol and dried in a vacuum oven at 50 °C for 0.5 h.

3.2.10 Coating of LB-MSNs on pH-sensitive microneedle arrays

To determine the level of binding of LB-MSNs on the microneedle arrays, DOPE-LR was added to the lipids when the LB-MSNs were prepared. The top of the microneedle arrays was incubated with LB-MSNs (50 µl) with a concentration of 0.1, 0.5 and 1 mg/mL in EDTA buffer (1 mM, pH 5.8) for 2 h at room temperature. The microneedles were then washed with coating buffer (450 µl) and the solution was kept for measurement. The binding efficiency of LB-MSNs was determined by comparing the DOPE-LR concentration in the coating solution before and after coating by using a Tecan M1000 plate reader (Excitation wavelength = 575 nm and Emission wavelength = 590 nm). The structure, geometry and the surface morphology of the LB-MSNs coated pH-sensitive microneedle arrays were examined by scanning electron microscopy (SEM) in a FEI NOVA nanoSEM 200. The LB-MSNs coated on microneedle arrays were also visualized by Nikon D-Eclipse C1 confocal laser scanning microscope (CLSM) with a depth resolution of 5 µm/step, equipped with a 10 × Plan Apo objective. The x and y resolution was 2.5 µm. An argon laser (488 nm) was used to visualize OVA-AF488 with a 530/55 emission filter and a diode-pumped solid-state laser (561 nm) with a 590/55 emission filter was used to visualize DOPE-LR.

3.2.11 Delivery of LB-MSNs from microneedles into ex vixo human skin

After coated with LB-MSNs, the pH-sensitive microneedles were pierced into abdomen human skin, which was used within 24 h after cosmetic surgery from a local hospital. The microneedles were applied into the skin by an impact-insertion applicator with a velocity of 54.8 cm/sec as described previously.[8] After 1 second, the applicator was removed and the microneedles were kept inside the skin for 30 min. Then the microneedles were removed and the skin was visualized by Nikon D-Eclipse C1 CLSM with a depth resolution of 5 µm/step, equipped with a 4 × Plan Apo objective. The x and y resolution was 6.3 µm. An argon laser (488 nm) was used to visualize OVA-AF488 with a 530/55 emission filter and a diode-pumped solid-state laser (561 nm) with a 590/55 emission filter was used to visualize DOPE-LR.

3.2.12 Statistical analysis

All data shown are mean corrected values ± SD of at least three experiments.

3.3 Results and discussion

For the efficient dermal delivery of proteins, nanoparticles are required that are small (diameter < 200 nm) and with large pores (inner diameter > 5 nm) in order to encapsulate large amounts of proteins. Most nanosized mesoporous silica nanoparticles do not fit these criteria and only recently some examples have emerged, mainly for the delivery of DNA/RNA.[35, 45-50] Therefore we synthesized a new type of large pore MSNs in order to encapsulate proteins with high efficiency. The MSNs were synthesized from the silica precursor tetraethoxy silane (TEOS) by using a mixture of a nonionic triblock copolymer (Pluronic P-123) and the cationic fluorocarbon surfactant (FC-4) as organic templates. Furthermore the swelling agent 1,3,5-trimethylbenzene (TMB) was added to induce the formation of large-pore MSNs.[38] The obtained pristine MSNs were modified with 3-[2-(2-aminoethylamino)ethylamino] propyltrimethoxysilane (AEPTMS) in order to create a positively charged surface (AEP-MSNs). Inspection with transmission electron microscopy (TEM) revealed that the prepared negatively charged MSNs were rectangular in shape with mesochannels along the short axis (Figure 3.1a). Modification with AEPTMS did not alter the morphology and mesostructure (Figure 3.1b), as compared to pristine MSNs. Furthermore, characterization with N_2 adsorption-desorption isotherms of both MSNs and AEP-MSNs showed that these nanoparticles have typical IV isotherms according to International Union of Pure and Applied Chemistry (IUPAC) classification (Figure 3.1c).[51] The existence of channel-type of mesopores was confirmed by the observed existence of a type-H_1 hysteresis loop (Figure 3.1c).[52] The values for Brunauer-Emmett-Teller (BET) specific surface area (S_{BET}), the total pore volume (V_t), Barrett-Joyner-Halenda (BJH) pore diameter (W_{BJH}) and surface charge of MSNs and AEP-MSNs are summarized in Table 3.1.

Table 3.1 Physical characteristics of MSNs and AEP-MSNs

Sample	BET surface area (m^2/g)	Pore volume (cm^3/g)	Pore diameter (nm)[a]	Zeta-potential (mV)[b]
MSNs	506	1.01	10 ± 1	-27.8 ± 0.4
AEP-MSNs	318	0.71	9 ± 1	10.9 ± 0.5

[a]Calculated from desorption branch of the N_2 sorption isotherms based on the BJH method.

[b]Zeta-potential was measured in 1 mM PB at pH 7.4.

It can be seen that after modification with AEPTMS, S_{BET}, V_t and W_{BJH} were slightly reduced because of the attachment of the functionalized silanes on the pore surface. The pore diameter of the AEP-MSNs was 1-2 nm smaller than that of MSNs (Figure 3.1c inset), but still sufficiently large to accommodate OVA (4 × 5 × 7 nm).[33] Dynamic light scattering (DLS) measurements showed that the hydrodynamic diameter of MSNs and AEP-MSNs was 146.3 ± 0.3 nm and 213.7 ± 0.8 nm with a low polydispersity index (PDI), respectively (Figure 3.1d). The observed increase in Z-average size for AEP-MSNs may be attributed to some particle aggregation, which is probably due to the decreased charge repulsion among AEP-MSNs compared to MSNs (Table 3.1).

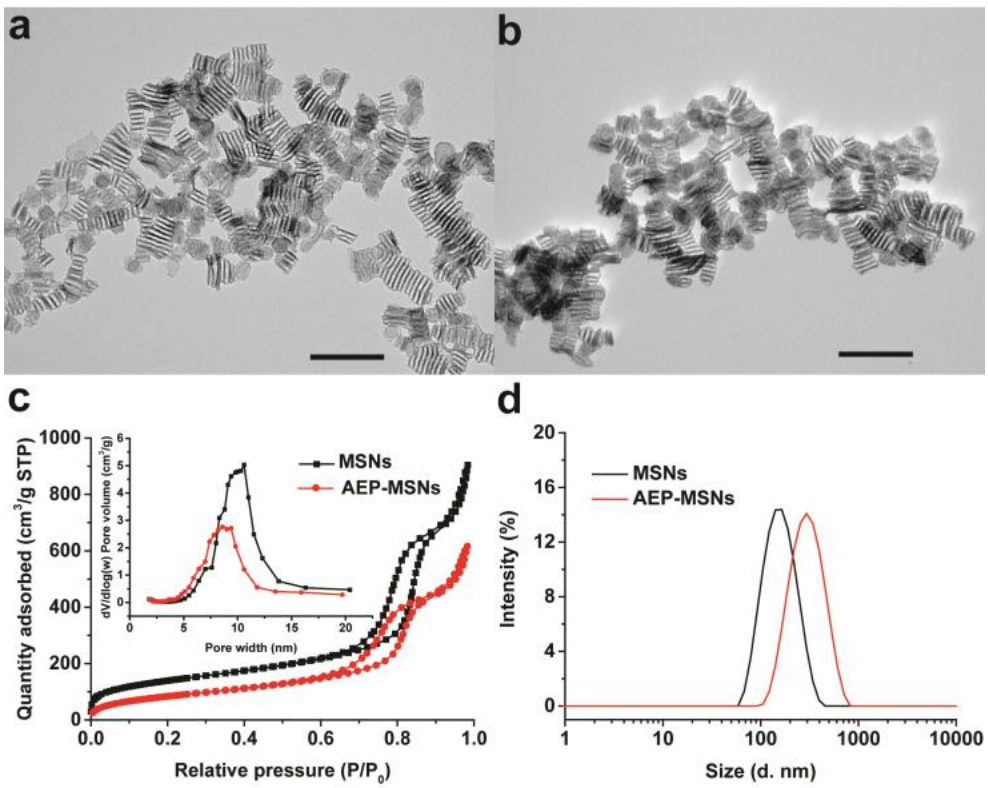

Figure 3.1 *Characterization of the MSNs and AEP-MSNs. TEM images of (a) MSNs and (b) AEP-MSNs. Scale bar = 200 nm. (c) Nitrogen adsorption-desorption isotherms and plots of pore diameter vs. pore volume (inset), calculated from the desorption isotherms using BJH model, show that the MSNs and AEP-MSNs have an average pore diameter of 10 nm and 9 nm, respectively. (d) Hydrodynamic diameter of MSNs and AEP-MSNs according to DLS.*

The percentage of graft amine-containing groups on the surface of AEP-MSNs was 6.9%, as determined by thermogravimetric analysis (TGA, see Figure 3.2a). The encapsulation efficiency (EE%), defined as the percentage of the protein OVA which is adsorbed in the MSNs or AEP-MSNs was determined as a function of incubation time (Figure 3.2b). This study revealed that the OVA encapsulation within AEP-MSNs was very efficient, as 94.83 ± 0.38% (mean ± SD, n = 3) of the protein was encapsulated in the AEP-MSNs. Furthermore, equilibrium of OVA encapsulation was reached in less than 5 min. In comparison, only 11.70 ± 2.23% (mean ± SD, n = 3) of OVA was encapsulated in negatively charged MSNs after 24 h. The loading capacity (LC%) of OVA was calculated from the amount of OVA encapsulated in AEP-MSNs and expressed as the percentage of the total weight of OVA loaded AEP-MSNs. The LC% of OVA in AEP-MSNs was dependent on the initial concentration of OVA (Figure 3.2c). The maximum LC% was about 33.94 ± 3.64% (mean ± SD, n = 3) by increasing the initial concentration of OVA, indicating a diffusion-driven encapsulation process.[53]

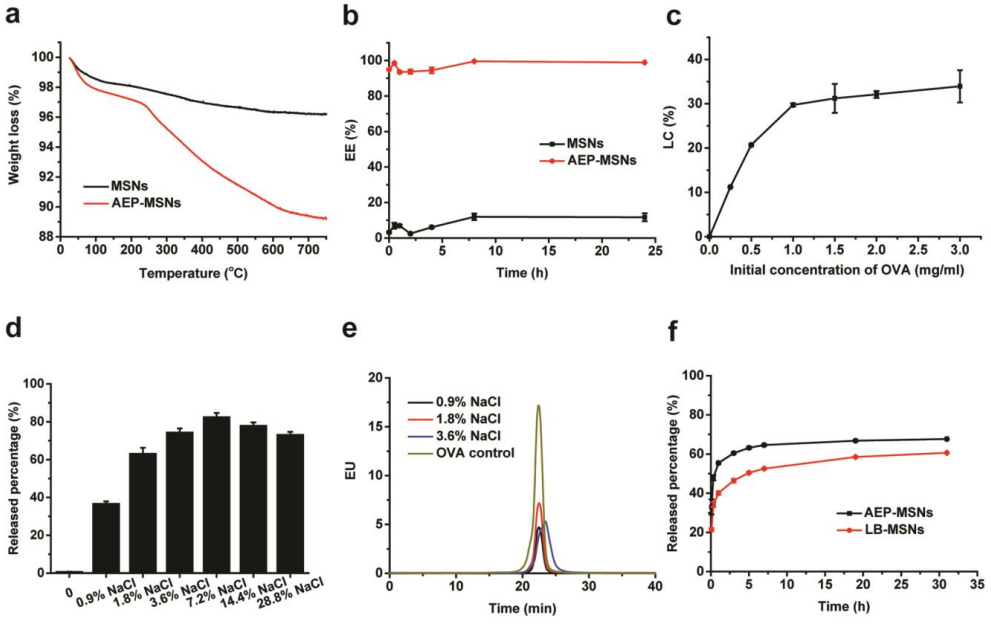

Figure 3.2 *(a) Thermogravimetric analysis (TGA) curves of MSNs and AEP-MSNs. (b) Encapsulation kinetics of OVA into MSNs and AEP-MSNs, concentration of OVA is 0.5 mg/mL and MSNs (AEP-MSNs) is 2 mg/mL. (c) Loading capacity (LC%) of OVA into AEP-MSNs at different initial concentration of OVA. (d) Influence of ionic strength on OVA release*

from AEP-MSNs. (e) HP-SEC chromatograms of the released OVA from AEP-MSNs. (f) OVA release profiles of OVA from AEP-MSNs and LB-MSNs in PBS (pH 7.4).

To examine the influence of ionic strength of the medium on the release profile of OVA from the AEP-MSNs, the concentration of NaCl in the buffer was varied. The release percentage of OVA (defined as the percentage of OVA released from total encapsulated OVA in AEP-MSNs) increased from 0.64 ± 0.16% (mean ± SD, n=3) in NaCl-free buffer to 82.40 ± 1.84% (mean ± SD, n = 3) in the buffer containing 7.2% NaCl (Figure 3.2d). These results demonstrate that the ionic strength of the medium plays an important role in the release of OVA, indicating that the interaction between OVA and AEP-MSNs is mainly of electrostatic nature. The structural integrity of the released OVA was examined by high pressure size-exclusion chromatography (HP-SEC), showing that the released OVA was mainly monomeric (Figure 3.2e), and far-UV circular dichroism (CD) spectroscopy, indicating that the secondary structure of released protein was similar to that of native OVA (Figure 3.S1). These results strongly indicate that encapsulation and release have no adverse effect on the protein structure.

The OVA-loaded AEP-MSNs had the tendency to precipitate and to form large aggregates, probably due to the decreased surface charge upon protein encapsulation (-8.1 ± 1.3 mV, mean ± SD, n = 3). In order to increase the colloidal stability, the OVA-loaded AEP-MSNs were therefore stabilized with a lipid bilayer composed of 1,2-dioleoyl-*sn*-glycero-3-phosphocholine (DOPC), 1,2-dioleoyl-*sn*-glycero-3-phospho-L-serine (DOPS) and cholesterol. For this, liposomes and OVA-loaded AEP-MSNs were mixed and equilibrated for 1.5 h and afterwards the excess of lipids was removed by centrifugation. The encapsulation efficiency of OVA in the resulting lipid coated AEP-MSNs (LB-MSNs) was determined to be 73.83 ± 0.74%, as compared to 98.88 ± 0.52% without lipid (mean ± SD, n = 3). The obtained LB-MSNs were characterized by dynamic light scattering (DLS), nanoparticle tracking analysis (NTA) and TEM. The mean number-based hydrodynamic diameter (176 ± 11 nm, mean ± SD, n = 3) measured by NTA (Figure 3.S2) was close to the Z-average hydrodynamic diameter (190.7 ± 2.7 nm; PDI = 0.125 ± 0.029; mean ± SD, n = 3) found by DLS (Figure 3.3a). The existence of a lipid layer surrounding the AEP-MSNs was confirmed by cryoTEM (Figure 3.3b,c). The colloidal stability of the formulation was examined by measuring the hydrodynamic diameter and zeta-potential of LB-MSNs for one week (Figure 3.S3). LB-MSNs showed only slight changes in diameter and zeta-potential revealing that the lipid bilayer strongly enhances the colloidal stability. The release of OVA from AEP-MSNs and LB-MSNs was examined in PBS (pH 7.4) for 32 h (Figure 3.2f). The burst release of OVA

from LB-MSNs was less as compared to AEP-MSNs, indicating that the lipid bilayer acts as a barrier retaining the OVA longer inside the AEP-MSNs.

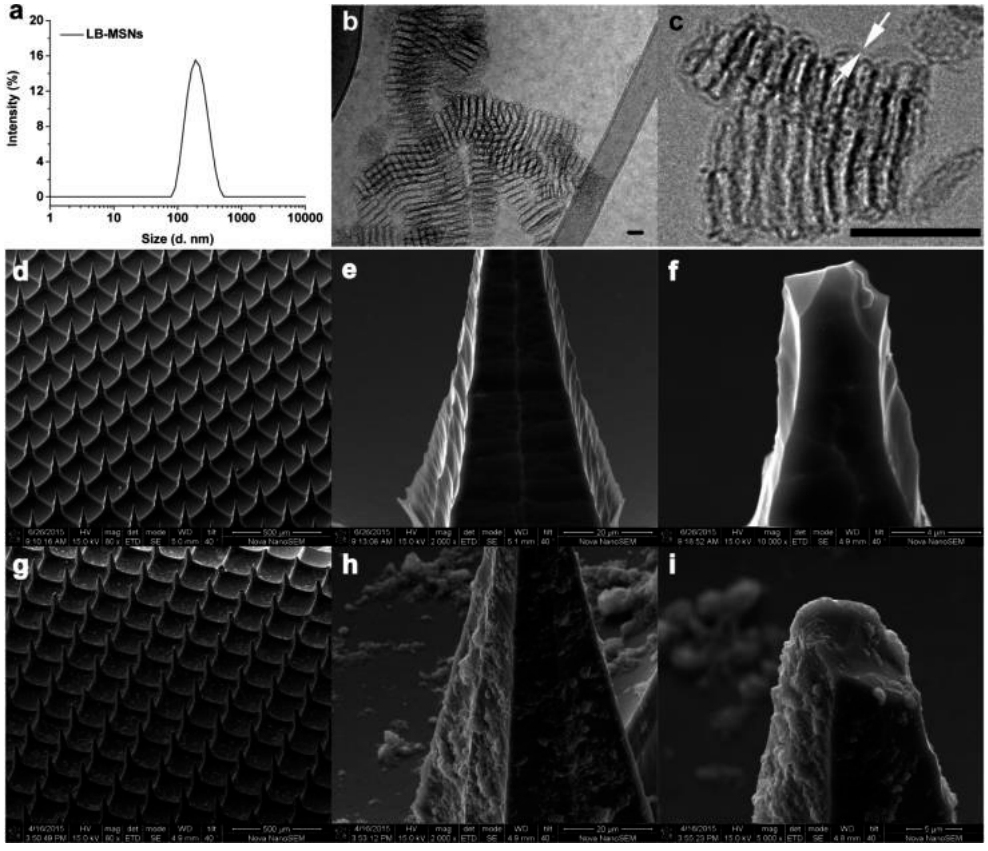

Figure 3.3 *(a) Hydrodynamic diameter of LB-MSNs determined by DLS. (b) Cryogenic TEM image of LB-MSNs, scale bar = 20 nm, (c) revealing a lipid bilayer thickness of ~4 nm, scale bar = 100 nm. (d-f) SEM images of pyridine-modified microneedle arrays before the adsorption of LB-MSNs with different magnifications (d: 80 ×; e: 2000 ×; f: 5000 ×). (g-i) SEM images of pyridine-modified microneedle arrays after the adsorption of LB-MSNs with different magnifications (g: 80 ×; h: 2000 ×; i: 5000 ×).*

Next, we investigated whether the LB-MSNs could be adsorbed to a silicon microneedle array via physical adsorption. First, the pH-sensitive pyridine-modified microneedle arrays were prepared as described previously.[8] LB-MSNs were coated onto these microneedle arrays at pH 5.8 in an ethylenediaminetetraacetic acid (EDTA) buffer (1 mM). At this pH more than 90% of the pyridine groups are positively charged.[8] Combined with the low ionic strength of the buffer, this allows for the binding of the negatively charged LB-MSNs via electrostatic

interactions. To determine the optimal concentration of LB-MSNs for the coating process, the nanoparticle concentration was varied in the buffered coating solution. Increasing the LB-MSN concentration resulted in increased amounts of LB-MSNs coated onto the microneedle array surfaces. However, the coating efficiency is reduced (Table 3.2). The lowest coating efficiency obtained was 15.82 ± 2.67 % (mean ± SD, n = 3), corresponding to 7.91 ± 1.34 μg (mean ± SD, n = 3) and 1.45 ± 0.24 μg (mean ± SD, n = 3) of LB-MSNs and OVA, respectively coated on the microneedles. Considering the surface area of the microneedles accounts for 40% of the total surface area of microneedle arrays, 3.16 ± 0.54 μg (mean ± SD, n = 3) of nanoparticles and 0.58 ± 0.10 μg (mean ± SD, n = 3) of OVA were coated onto the microneedle surface of one array.

Table 3.2 Coating amount of LB-MSNs and OVA on microneedle arrays

Amount of LB-MSNs[a] (μg)	Coated LB-MSNs (μg)	Coated OVA[b] (μg)	Coating efficiency (%)
5	1.33 ± 0.18	0.24 ± 0.03	26.58 ± 2.91
25	5.39 ± 1.70	0.99 ± 0.31	21.56 ± 6.79
50	7.91 ± 1.34	1.45 ± 0.24	15.82 ± 2.67

[a]The amount of LB-MSNs in coating solution; [b]The amount of coated OVA was calculated from the loading capacity of OVA and the coating amount of LB-MSNs. All the coating amounts are expressed as the amount of AEP-MSNs and are based on one microneedle array which contains 576 needles per array. All the results are based on 3 independent microneedle arrays.

Scanning electron microscopy (SEM) imaging was used to visualize the presence of the LB-MSNs on the pyridine modified microneedle arrays (Figure 3.3d-i). Compared to untreated pyridine-modified arrays (Figure 3.3d-f), a high number of nanoparticles were observed on the surface of the microneedles (Figure 3.3g-i) after coating with LB-MSNs. To determine whether the OVA and nanoparticles colocalized on the microneedles, the LB-MSNs coated microneedles were visualized by confocal laser scanning microscopy (CLSM). For this experiment, we used Alexa Fluor®488 labeled ovalbumin (OVA-AF488) and 1,2-dioleoyl-sn-glycero-3-phosphoethanolamine-N-(lissamine rhodamine B sulfonyl) (ammonium salt) (DOPE-LR) enabling the visualization of both the protein and lipids. Imaging revealed that the fluorescent labels were both located at the microneedle surfaces indicative of the integrity of the LB-MSNs upon physical adsorption (Figure 3.4a-c). This showed us that LB-MSNs could be immobilized onto microneedles via electrostatic interaction.

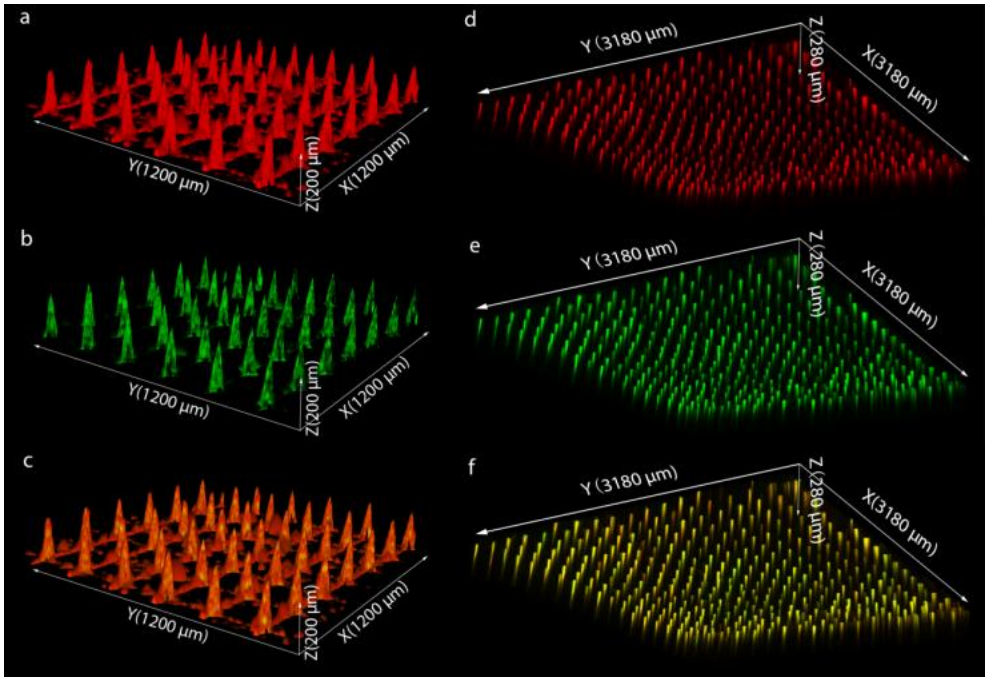

Figure 3.4 *Confocal laser scanning microscopy (CLSM) images of LB-MSN coated microneedles (a-c). Red: DOPE-LR (a); Green: OVA-AF488 (b); Merged (c). The x and y arrows show that the scanning area is 1200 µm × 1200 µm large. The z arrow indicates the scanning depth of 200 µm. CLSM images after removal of the LB-MSN coated microneedle arrays (d-f). Red: DOPE-LR (d); Green: OVA-AF488 (e); Merged (f). The x and y arrows show that the scanning area is 3180 µm × 3180 µm large. The z arrow indicates the scanning depth of 280 µm.*

Next, the delivery of LB-MSNs from the surface of microneedles into the skin was studied. For this, the nanoparticle-coated microneedle arrays were applied onto human skin *ex vivo* for 30 min and subsequently withdrawn. Next the intradermal delivery was studied, colocalization of the fluorescence from both OVA-AF488 and DOPE-LR was observed inside the skin (Figure 3.4d-f), illustrating that the microneedles penetrated into the skin and successfully delivered the LB-MSNs.

3.4 Conclusion

LB-MSNs based nanoparticles with large (10 nm) pores represent a novel biocompatible carrier for dermal antigen delivery. The large pores enabled the rapid encapsulation of OVA with a high loading capacity. The introduction of lipid bilayers significantly improved the colloidal stability of OVA loaded AEP-MSNs and concomitantly reduced the premature release of OVA. In addition, it enabled the coating of the nanoparticles on the surface of pH-sensitive microneedle arrays. Application of LB-MSNs coated microneedle arrays into human skin (*ex vivo*) resulted in the successful delivery of the OVA loaded nanoparticles into the skin. This is the first example of a microneedle-mediated intradermal delivery system for mesoporous nanoparticles, which could be a promising tool to deliver a wide range of compounds into the skin. The method is not restricted to the delivery of antigens, but can also be used to deliver any compound that can be encapsulated in MSNs like (low-molecular-weight) drugs, RNA/DNA and proteins.[54, 55]

Supporting Information

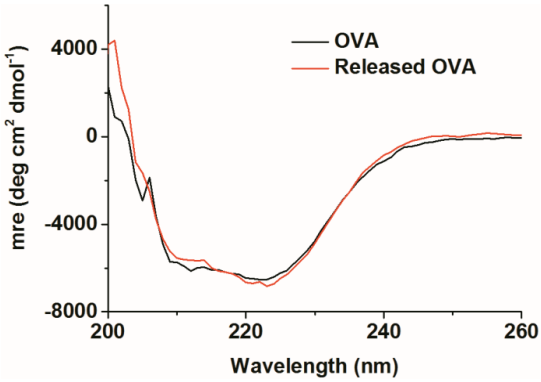

Figure 3.S1 *Far-UV CD spectra of free OVA and OVA released from AEP-MSNs in PBS, pH 7.4, 25 °C.*

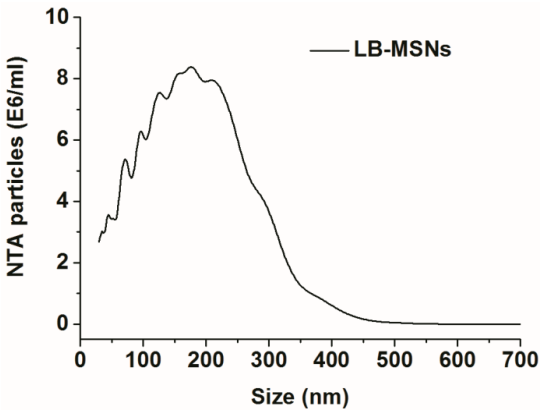

Figure 3.S2 *Size distribution of the LB-MSNs determined by nanoparticle tracking analysis (NTA).*

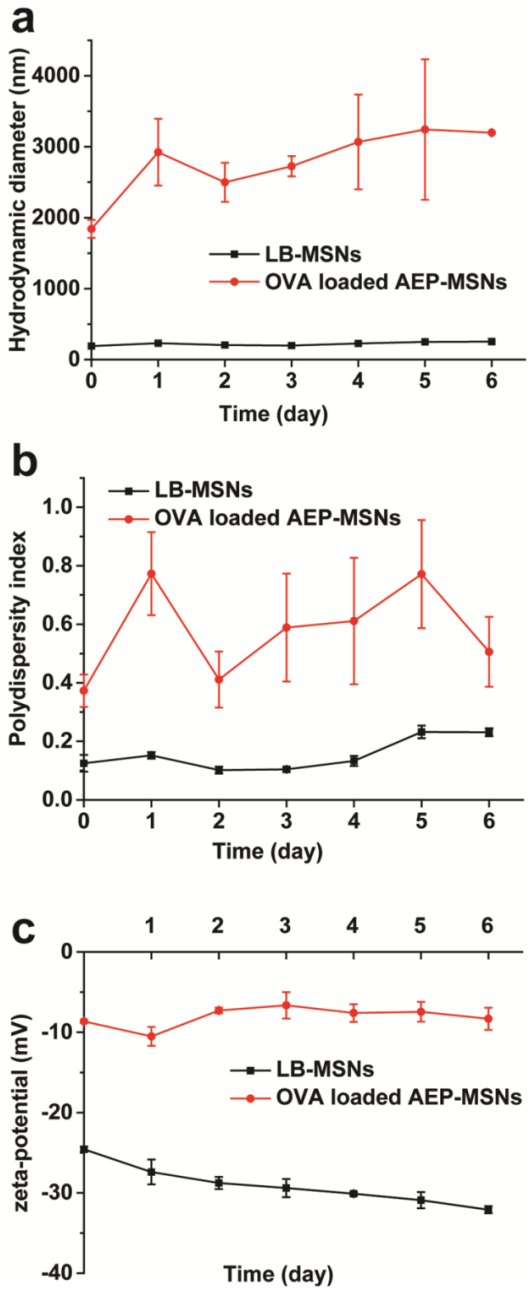

Figure 3.S3 *Colloidal stability of LB-MSNs (black curve) and OVA loaded AEP-MSNs (red curve) as a function of time, measured in 1 mM PB, pH 7.4. (a) Hydrodynamic diameter and (b) polydispersity index (PDI), both determined by DLS (the results of OVA loaded AEP-MSNs do not meet quality criteria), and (c) zeta-potential, determined by laser Doppler electrophoresis.*

3.5 References

1. Y. B. Deng, R. Mathaes, G. Winter and J. Engert, *Eur. J. Pharm. Sci.*, **2014**, 63, 154-166.
2. K. T. Mody, A. Popat, D. Mahony, A. S. Cavallaro, C. Yu and N. Mitter, *Nanoscale*, **2013**, 5, 5167-5179.
3. C. Wang, Y. Ye, G. M. Hochu, H. Sadeghifar and Z. Gu, *Nano Lett.*, **2016**, 16, 2334-2340.
4. K. van der Maaden, W. Jiskoot and J. Bouwstra, *J. Controlled Release*, **2012**, 161, 645-655.
5. K. van der Maaden, E. Sekerdag, W. Jiskoot and J. Bouwstra, *AAPS J.*, **2014**, 16, 681-684.
6. P. C. Demuth, W. F. Garcia-Beltran, M. L. Ai-Ling, P. T. Hammond and D. J. Irvine, *Adv. Funct. Mater.*, **2013**, 23, 161-172.
7. S. M. Bal, B. Slutter, E. van Riet, A. C. Kruithof, Z. Ding, G. F. A. Kersten, W. Jiskoot and J. A. Bouwstra, *J. Controlled Release*, **2010**, 142, 374-383.
8. K. van der Maaden, H. Yu, K. Sliedregt, R. Zwier, R. Leboux, M. Oguri, A. Kros, W. Jiskoot and J. A. Bouwstra, *J. Mater.Chem. B*, **2013**, 1, 4466-4477.
9. S. H. Lee, H. H. Lee and S. S. Choi, *Korean J. Chem. Eng.*, **2011**, 28, 1913-1917.
10. X. Wang, N. Wang, N. Li, Y. Zhen and T. Wang, *Hum. Vaccines Immunother.*, **2016**, 1-15.
11. K. van der Maaden, K. Sliedregt, A. Kros, W. Jiskoot and J. Bouwstra, *Langmuir*, **2012**, 28, 3403-3411.
12. W. Zhang, J. Gao, Q. G. Zhu, M. Zhang, X. Y. Ding, X. Y. Wang, X. M. Hou, W. Fan, B. Y. Ding, X. Wu, X. Y. Wang and S. Gao, *Int. J. Pharm.*, **2010**, 402, 205-212.
13. P. C. DeMuth, X. F. Su, R. E. Samuel, P. T. Hammond and D. J. Irvine, *Adv. Mater.*, **2010**, 22, 4851-4856.
14. S. A. Coulman, A. Anstey, C. Gateley, A. Morrissey, P. McLoughlin, C. Allender and J. C. Birchall, *Int. J. Pharm.*, **2009**, 366, 190-200.
15. M. Zaric, O. Lyubomska, C. Poux, M. L. Hanna, M. T. McCrudden, B. Malissen, R. J. Ingram, U. F. Power, C. J. Scott, R. F. Donnelly and A. Kissenpfennig, *J. Invest. Dermatol.*, **2015**, 135, 425-434.
16. L. Guo, J. Chen, Y. Qiu, S. Zhang, B. Xu and Y. Gao, *Int. J. Pharm.*, **2013**, 447, 22-30.
17. M. Zaric, O. Lyubomska, O. Touzelet, C. Poux, S. Al-Zahrani, F. Fay, L. Wallace, D. Terhorst, B. Malissen, S. Henri, U. F. Power, C. J. Scott, R. F. Donnelly and A. Kissenpfennig, *ACS Nano*, **2013**, 7, 2042-2055.
18. P. C. DeMuth, J. J. Moon, H. Suh, P. T. Hammond and D. J. Irvine, *ACS Nano*, **2012**, 6, 8041-8051.
19. Y. Zhuang, Y. Ma, C. Wang, L. Hai, C. Yan, Y. Zhang, F. Liu and L. Cai, *J. Controlled Release*, **2012**, 159, 135-142.
20. R. De Rose, A. N. Zelikin, A. P. R. Johnston, A. Sexton, S. F. Chong, C. Cortez, W. Mulholland, F. Caruso and S. J. Kent, *Adv. Mater.*, **2008**, 20, 4698-4703.
21. J. C. Aguilar and E. G. Rodriguez, *Vaccine*, **2007**, 25, 3752-3762.
22. R. A. Rosalia, L. J. Cruz, S. van Duikeren, A. T. Tromp, A. L. Silva, W. Jiskoot, T. de Gruijl, C. Lowik, J. Oostendorp, S. H. van der Burg and F. Ossendorp, *Biomaterials*, **2015**, 40, 88-97.
23. D. Mahony, A. S. Cavallaro, F. Stahr, T. J. Mahony, S. Z. Qiao and N. Mitter, *Small*, **2013**, 9, 3138-3146.
24. A. A. Hwang, J. Lu, F. Tamanoi and J. I. Zink, *Small*, **2015**, 11, 319-328.
25. F. Porta, G. E. M. Lamers, J. Morrhayim, A. Chatzopoulou, M. Schaaf, H. den Dulk, C. Backendorf, J. I. Zink and A. Kros, *Adv. Healthcare Mater.*, **2013**, 2, 281-286.
26. H. Meng, M. Xue, T. Xia, Z. X. Ji, D. Y. Tarn, J. I. Zink and A. E. Nel, *ACS Nano*, **2011**, 5, 4131-4144.
27. S. H. van Rijt, D. A. Bölükbas, C. Argyo, S. Datz, M. Lindner, O. Eickelberg, M. Königshoff, T. Bein and S. Meiners, *ACS Nano*, **2015**, 9, 2377-2389.
28. C. Argyo, V. Weiss, C. Bräuchle and T. Bein, *Chem. Mater.*, **2014**, 26, 435-451.
29. E. Aznar, M. Oroval, L. Pascual, J. R. Murguia, R. Martinez-Manez and F. Sancenon, *Chem. Rev.*, **2016**, 116, 561-718.
30. H. Meng, Y. Zhao, J. Y. Dong, M. Xue, Y. S. Lin, Z. X. Ji, W. X. Mai, H. Y. Zhang, C. H. Chang, C. J. Brinker, J. I. Zink and A. E. Nel, *ACS Nano*, **2013**, 7, 10048-10065.

31. F. Sharif, F. Porta, A. H. Meijer, A. Kros and M. K. Richardson, *Int. J. Nanomed.*, **2012**, 7, 1875-1890.
32. J. Tu, T. Wang, W. Shi, G. Wu, X. Tian, Y. Wang, D. Ge and L. Ren, *Biomaterials*, **2012**, 33, 7903-7914.
33. S. Hudson, J. Cooney and E. Magner, *Angew. Chem., Int. Ed.*, **2008**, 47, 8582-8594.
34. E. C. Dengler, J. W. Liu, A. Kerwin, S. Torres, C. M. Olcott, B. N. Bowman, L. Armijo, K. Gentry, J. Wilkerson, J. Wallace, X. M. Jiang, E. C. Carnes, C. J. Brinker and E. D. Milligan, *J. Controlled Release*, **2013**, 168, 209-224.
35. K. Epler, D. Padilla, G. Phillips, P. Crowder, R. Castillo, D. Wilkinson, B. Wilkinson, C. Burgard, R. Kalinich, J. Townson, B. Chackerian, C. Willman, D. Peabody, W. Wharton, C. J. Brinker, C. Ashley and E. Carnes, *Adv. Healthcare Mater.*, **2012**, 1, 348-353.
36. C. E. Ashley, E. C. Carnes, K. E. Epler, D. P. Padilla, G. K. Phillips, R. E. Castillo, D. C. Wilkinson, B. S. Wilkinson, C. A. Burgard, R. M. Kalinich, J. L. Townson, B. Chackerian, C. L. Willman, D. S. Peabody, W. Wharton and C. J. Brinker, *ACS Nano*, **2012**, 6, 2174-2188.
37. C. E. Ashley, E. C. Carnes, G. K. Phillips, D. Padilla, P. N. Durfee, P. A. Brown, T. N. Hanna, J. Liu, B. Phillips, M. B. Carter, N. J. Carroll, X. Jiang, D. R. Dunphy, C. L. Willman, D. N. Petsev, D. G. Evans, A. N. Parikh, B. Chackerian, W. Wharton, D. S. Peabody and C. J. Brinker, *Nat. Mater.*, **2011**, 10, 389-397.
38. Y. Han and J. Y. Ying, *Angew. Chem., Int. Ed.*, **2005**, 44, 288-292.
39. J. B. Tu, A. L.; Friedrich,H.; Bomans, P. H. H.; Bussmann,J.; Sommerdijk, N. A. J. M.; Wim Jiskoot, W.; Kros, A., **2016**.
40. X. B. Zhao, L. Liu, X. R. Li, J. Zeng, X. Jia and P. Liu, *Langmuir*, **2014**, 30, 10419-10429.
41. S. Brunauer, P. H. Emmett and E. Teller, *J. Am. Chem. Soc.*, **1938**, 60, 309-319.
42. E. P. Barrett, L. G. Joyner and P. P. Halenda, *J. Am. Chem. Soc.*, **1951**, 73, 373-380.
43. H. Friedrich, P. M. Frederik, G. de With and N. A. J. M. Sommerdijk, *Angew. Chem., Int. Ed.*, **2010**, 49, 7850-7858.
44. K. van der Maaden, H. X. Yu, K. Sliedregt, R. Zwier, R. Leboux, M. Oguri, A. Kros, W. Jiskoot and J. A. Bouwstra, *J. Mater.Chem. B*, **2013**, 1, 4466-4477.
45. K. Moller, K. Muller, H. Engelke, C. Brauchle, E. Wagner and T. Bein, *Nanoscale*, **2016**, 8, 4007-4019.
46. N. Z. Knezevic and J.-O. Durand, *Nanoscale*, **2015**, 7, 2199-2209.
47. H. K. Na, M. H. Kim, K. Park, S. R. Ryoo, K. E. Lee, H. Jeon, R. Ryoo, C. Hyeon and D. H. Min, *Small*, **2012**, 8, 1752-1761.
48. X. Du, L. Xiong, S. Dai, F. Kleitz and S. Z. Qiao, *Adv. Funct. Mater.*, **2014**, 24, 7627-7637.
49. S. B. Hartono, N. T. Phuoc, M. H. Yu, Z. F. Jia, M. J. Monteiro, S. H. Qiao and C. Z. Yu, *J. Mater.Chem. B*, **2014**, 2, 718-726.
50. D. S. Lin, Q. Cheng, Q. Jiang, Y. Y. Huang, Z. Yang, S. C. Han, Y. N. Zhao, S. T. Guo, Z. C. Liang and A. J. Dong, *Nanoscale*, **2013**, 5, 4291-4301.
51. B. L. Zhang, Z. Luo, J. J. Liu, X. W. Ding, J. H. Li and K. Y. Cai, *J. Controlled Release*, **2014**, 192, 192-201.
52. J. Sun, H. Zhang, R. Tian, D. Ma, X. Bao, D. S. Su and H. Zou, *Chem. Commun.*, **2006**, 1322-1324.
53. I. I. Slowing, B. G. Trewyn and V. S. Y. Lin, *J. Am. Chem. Soc.*, **2007**, 129, 8845-8849.
54. Q. J. He and J. L. Shi, *Adv. Mater.*, **2014**, 26, 391-411.
55. F. Q. Tang, L. L. Li and D. Chen, *Adv. Mater.*, **2012**, 24, 1504-1534.